

OLA-VLM: Elevating Visual Perception in Multimodal LLMs with Auxiliary Embedding Distillation

Jitesh Jain^{1,2*}, Zhengyuan Yang², Humphrey Shi^{1†}, Jianfeng Gao^{2†}, Jianwei Yang^{2†}

¹SHI Labs @ Georgia Tech, ²Microsoft Research, Redmond

<https://github.com/SHI-Labs/OLA-VLM>

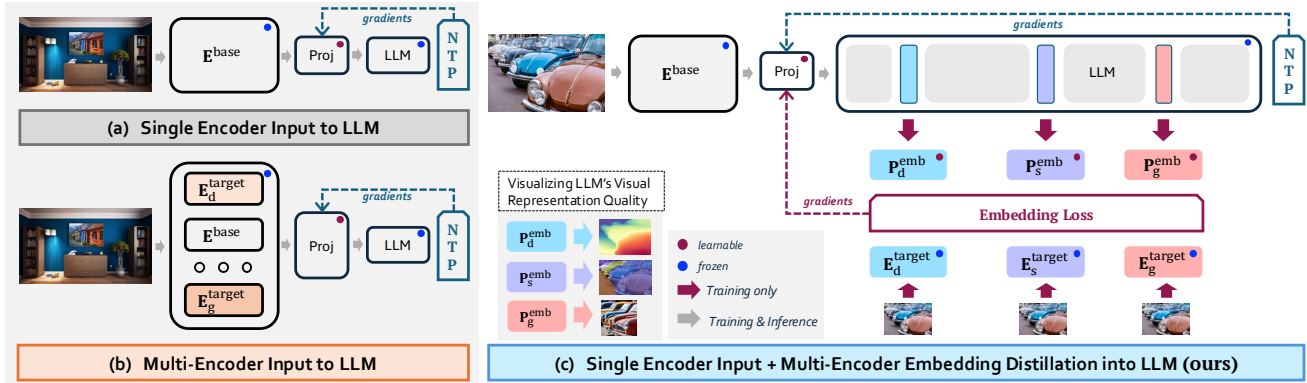


Figure 1. **Different Paradigms for Incorporating Visual Information into LLMs.** (a, b) Existing approaches [1, 41, 61] feed features from the visual encoder(s) into the LLM and train the model solely with natural language supervision, i.e., next (text) token prediction (NTP) objective to align the embedding space of the vision encoder(s) and the LLM. (c) We propose distilling target visual information into the intermediate representations of the LLM from a set of target encoders (E^{target}). We adopt a predictive embedding [2, 4] optimization approach at selected LLM layers during training to minimize the embedding losses along with the next token prediction (NTP) objective loss function, resulting in a vision-centric approach to training the Multimodal Large Language Model. We only use a single base vision encoder during inference.

Abstract

The standard practice for developing contemporary MLLMs is to feed features from vision encoder(s) into the LLM and train with natural language supervision. In this work, we posit an overlooked opportunity to optimize the intermediate LLM representations through a vision perspective (objective), i.e., solely natural language supervision is sub-optimal for the MLLM’s visual understanding ability. To that end, we propose **OLA-VLM**, the first approach distilling knowledge into the LLM’s hidden representations from a set of target visual representations. Firstly, we formulate the objective during the pretraining stage in MLLMs as a coupled optimization of predictive visual embedding and next text-token prediction. Secondly, we investigate MLLMs trained solely with natural language supervision and identify a positive correlation between the quality of visual representations within these models and their down-

stream performance. Moreover, upon probing our OLA-VLM, we observe improved representation quality owing to the embedding optimization. Thirdly, we demonstrate that our OLA-VLM outperforms the single and multi-encoder baselines, proving our approach’s superiority over explicitly feeding the corresponding features to the LLM. Particularly, OLA-VLM boosts performance by an average margin of up to 2.5% on various benchmarks, with a notable improvement of 8.7% on the Depth task in CV-Bench.

1. Introduction

In the last couple of years, open-source Multimodal Large Language Models (MLLMs) [35, 41, 75] development has witnessed rapid growth, owing mainly to the increasing number of powerful LLMs [17, 58–60, 62] and large-scale datasets [11, 61, 64, 73]. The established practice to improve MLLMs at visual understanding tasks is training on increasing data with solely natural language supervision, i.e., a next text token prediction objective [34, 48, 61]. Re-

*Work done during JJ’s internship at MSR.

†Equal advising.

regardless of the data quantity, training an MLLM involves two primary stages: (i) Pre-Training (PT), aligning embeddings from vision encoder(s) to those inside the LLM, and (ii) Instruction Fine-Tuning (IFT), training the model on conversation data for downstream instruction following tasks. However, solely using natural language supervision during training does not guarantee the optimal quality of visual representations inside the LLM. To counter this issue, a few works propose simply scaling the number of visual (input) encoders [21, 31, 32, 37, 42, 56, 61], or using visual cross-attention [1, 15] inside the LLM, leading to high compute and data costs for convergence during training. In this work, we posit that solely using natural language supervision for scaling MLLMs with more data, visual inputs, or network components often overlooks a hidden opportunity to optimize the visual quality of representations inside the LLM directly. To that end, we propose to distill knowledge from a set of teacher visual encoders into the LLM’s representations during the PT stage through a set of embedding losses (Fig. 1c). During inference, we only use a single encoder, resulting in a better trade-off between visual understanding performance and efficiency as compared to explicitly feeding (multiple) visual inputs to the LLM (Fig. 1a,b).

Before experimenting with our embedding losses, we train a probe for the representations from each layer inside the LLM (of the MLLM, LLaVA-1.5 [41], in our case) to analyze their quality against the target visual features. We choose features from visual encoders trained for three tasks as targets: image segmentation [29, 30, 33, 52, 76], depth estimation [69, 70] and image generation [50, 53], owing to their well-studied, fundamental nature and the first two being seminal perception abilities [20, 25]. Specifically, we train the probes for each task to predict the corresponding target encoder’s output. We find that the probing performance gradually improves with more data, indicating that the LLM enhances its visual understanding ability and, consequently, downstream performance, proving the effectiveness of our probing setup, as shown in Fig. 2a. Moreover, we establish that the middle LLM layers are optimal for embedding visual information inside the LLM based on the layer-wise trend for the probes’ performance. We provide more details about our probing setup in Sec. 3.

With the knowledge regarding the nature of the different layers from the probing experiments, we investigate the effect of optimizing the information from the corresponding target encoders in the intermediate LLM representations. Inspired by the recent works in embedding predictive architectures for self-supervised learning [2, 26], we propose **OLA-VLM** to distill [27] knowledge from the target encoders into the LLM’s representation space. Specifically, we optimize an embedding loss between the target feature and the embedding predictor output at the corresponding LLM layer (Fig. 1c). Note that we still use features from

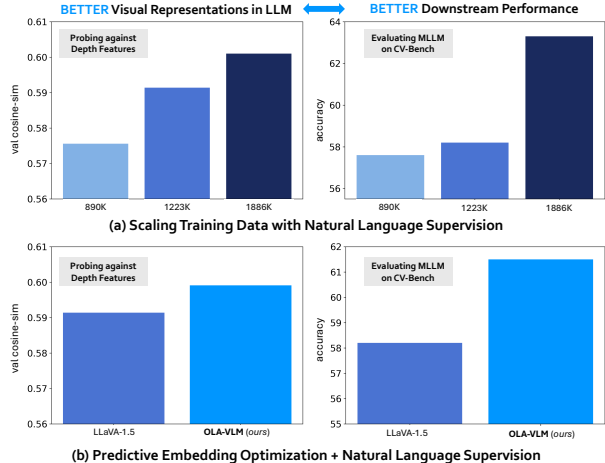


Figure 2. **Probing reveals a relationship between representation quality and performance.** (a) We observe that increasing the amount of data and training solely with the next-token prediction objective enhances the visual representation quality within the LLM, resulting in improved performance, underscoring the effectiveness of our probing setup. (b) Our **OLA-VLM** exhibits superior visual representations and performance compared to LLaVA-1.5 [41] under the same settings, demonstrating the effectiveness of minimizing the predictive embedding objective during training.

a base encoder as inputs to the language model. Furthermore, we incorporate a specialized set of tokens, $\langle t \rangle$, enriched with target-specific information into the LLM’s input sequence, fostering an implicit visual chain of thought and enhancing the model’s ability to handle target information-friendly queries. We hypothesize that optimizing the embeddings during the PT stage results in OLA-VLM outperforming the baselines owing to a better initialization of the (MLP) projector for the IFT stage. We validate the hypothesis in Sec. 3 using probes for our OLA-VLM, demonstrating improved performance in the initial LLM layers, indicating a more effective projection of vision features. Our experiments in Sec. 5 illustrate the effectiveness of our embedding optimization and special tokens, $\langle t \rangle$, on various benchmarks while outperforming the baselines under the same settings.

To summarize, our contributions are as follows:

- To the best of our knowledge, ours is the first study to analyze the quality of visual representations inside MLLMs. We probe the LLM layers in LLaVA-1.5 [41] based models and present our findings about enhancing MLLM’s visual understanding ability with increasing training data and layer index.
- We present **OLA-VLM**, the first approach to distill knowledge from target encoders into language model representations through predictive embedding optimization. Furthermore, we integrate tokens enriched with target information into the input sequence, resulting in an implicit visual chain-of-thought technique.
- We conduct extensive experiments to demonstrate the

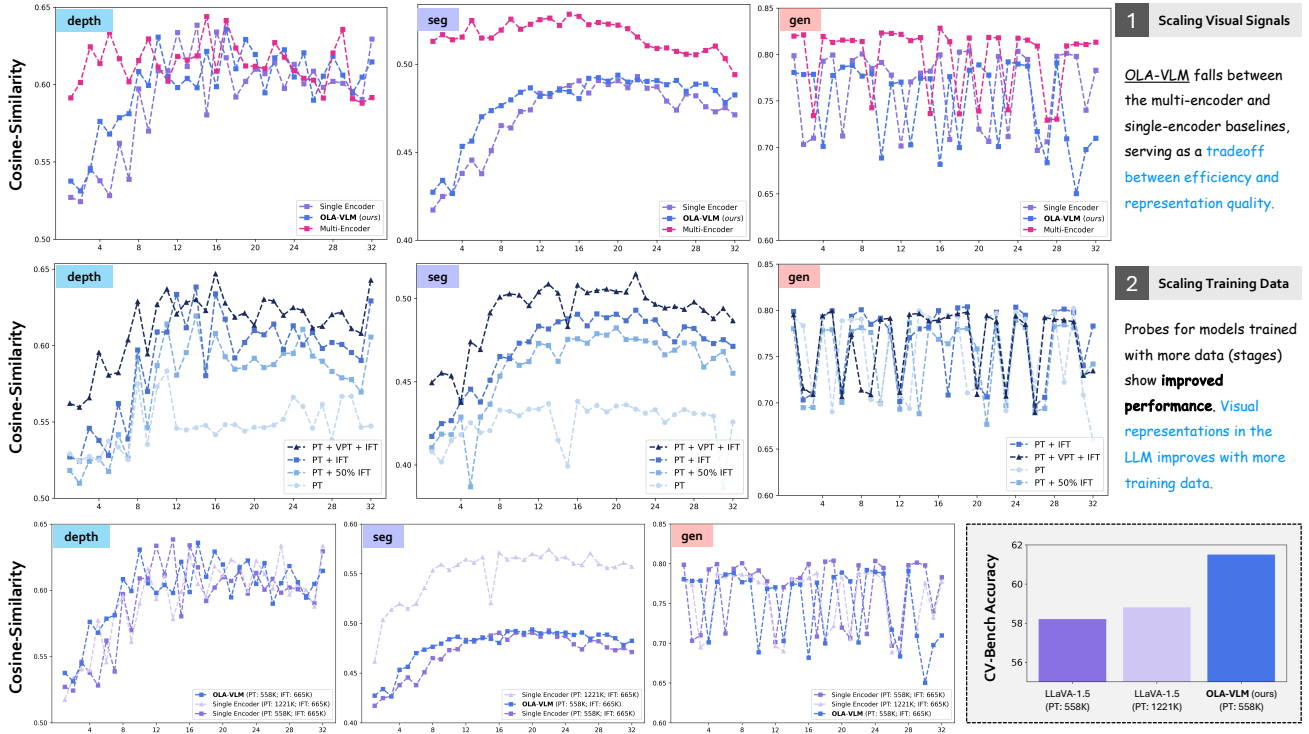


Figure 3. **Probing Visual Representations across LLM layers in Multimodal Large Language Models.** (1) As shown in the first row, the multi-encoder baseline has the best probing performance owing to the additional feature inputs. The performance of probes trained on our OLA-VLM falls between the two baselines, demonstrating the effectiveness of our embedding distillation approach in learning an improved projector while only using a single encoder during inference. (2) We observe that the probing performance for single encoder models trained solely with natural language supervision improves as the training data of the base MLLM increases, indicating that the LLM improves its visual representations of the world with more training data. In the last row, we observe that our OLA-VLM (base setting) outperforms the LLaVA-1.5 model trained with more data during the PT stage, demonstrating the effectiveness of our approach.

improvements of our proposed approach over the corresponding single and multi-encoder baselines on various benchmarks, including 8.7% and 5.6% on the Depth and Distance task on CV-Bench, respectively.

2. Related Works

2.1. MLLMs for Visual Reasoning

Contemporary MLLMs have three primary components: vision encoder(s), projector, and LLM.

One line of work [5, 22, 34, 35, 40, 41, 75] uses a single pretrained vision encoder [13, 19, 33, 44, 49, 72] and trains a projector, like an MLP [41] or QFormer [14] to align the vision encoder features with the LLM. A few recent approaches [18, 57] attempt to develop native MLLMs by directly feeding image patches into the LLM without using any pre-trained encoder. Some works [1, 15, 64, 68] train visual experts or cross-attention modules inside the LLM to disentangle visual and language information inside the LLM, often requiring millions of training data samples. We choose CLIP-ViT-L and CLIP-ConvNeXT-XXL as the base vision encoders for our experiments.

Another line of work explores using either multiple encoder features [37, 55, 61, 74] or multiple visual modalities [12, 31, 42] as inputs to the LLM for improved visual (spatial) reasoning performance. Our approach uses a single base vision encoder while embedding information from multiple encoder features into the LLM at different layers.

2.2. Probing Foundational Models

OthelloGPT [36] probed the features from a GPT-2 [48] trained on sequences from a board game, Othello, and found that the probes were able to learn the board state, indicating the ability of sequence models to learn world representations. A recent work probes the features from foundational vision encoders [3] for 3D tasks. In our work, we probe the embeddings from the LLM (of an MLLM) layers against target visual features. To the best of our knowledge, we are the first to establish a relationship between visual representations quality inside the MLLM and their performance.

2.3. Self-Supervised Learning

Distilling information [27] from a target encoder into a source encoder is a well-established technique to improve

the source encoder’s embeddings for a downstream task [8, 9, 24]. Recently, I-JEPA [2, 4] proposed an embedding predictive architecture to improve representations inside a source encoder by comparing the target encoder features and mapped source encoder features with a trained predictor. A concurrent work, REPA [71] improved DiTs [47] at image generation by distilling information from DINOv2 [16, 46]. Recently, a few works [51, 65] first distill information from target encoders into a single model and then leverage the resulting model as the vision encoder in an MLLM. Unlike previous works, we distill information from multiple vision encoders into the LLM embedding space during pre-training using image-text pairs, resulting in a more vision-centric MLLM training approach.

3. Visually Probing Language Embeddings

In this work, we aim to improve the representations inside the LLM with features from target encoders. However, first, we methodically analyze the quality of such features inside the LLM (of the MLLM) through probing. We choose encoders trained for three visual tasks as targets: image segmentation, depth estimation, and image generation. Our choice is guided by their fundamental and interpretable nature, i.e., visualizing the embedding representations’ quality through the respective task decoders. We use the encoders from Swin-L OneFormer [29, 43], DINOv2-L Depth Anything-v2 [19, 70], and ViT-L unCLIP-SD-2.1 [19, 49, 50, 53] as the segmentation (\mathbf{E}^{seg}), depth ($\mathbf{E}^{\text{depth}}$) and generation (\mathbf{E}^{gen}) encoders to obtain the target features for probing, respectively.

Our probing setup is quite simple. We train a single-layer Perceiver Resampler [28] as the probe head at every layer of the LLM of an MLLM model for each of the three target task features. We use a resampler probe head to accommodate the different sequence lengths of the target features and representations inside the LLM. The architecture of the probe head is similar to that of the Emb Predictor shown in Fig. 4. We input set of learnable latent queries for each layer’s probe head while using tokens from the corresponding layer as keys for cross-attention inside the resampler block. During training, we set the learning rate as $1e^{-3}$ for the probes and minimize the smooth-L1-loss objective with a batch size of 256. We train the probes for two epochs on the 118k images from the COCO-train2017 [38] set with the text query as “Describe the image in two lines.”. We analyze the following LLaVA-1.5 models with LLaMA-3-8b [58] as the decoder LLM and CLIP-ConvNeXT-XXL [13, 44] as the base encoder:

- **Single-Encoder MLLM** with features from \mathbf{E}^{base} passed through an MLP into the LLM.
- **Multi-Encoder MLLM** with features from \mathbf{E}^{base} , \mathbf{E}^{gen} , $\mathbf{E}^{\text{depth}}$, and \mathbf{E}^{seg} concatenated in the feature dimension (in order) and passed through an MLP into the LLM.

- **OLA-VLM** with features from \mathbf{E}^{base} passed through an MLP into the LLM and information from \mathbf{E}^{gen} , $\mathbf{E}^{\text{depth}}$, and \mathbf{E}^{seg} distilled into the LLM representations.

For evaluating a probe, we compute the cosine similarity between the probe outputs and the corresponding target features over the 5k images from the COCO-val2017 [38] set. For example, for a probe trained against the depth representations, we calculate the cosine similarity between the depth probe output and features from $\mathbf{E}^{\text{depth}}$ to get the probing performance at each layer.

Layerwise Trend. Upon evaluating the probes in the single encoder baseline, we observe an interesting trend that the middle (12-24) layer probes show the best representation quality for the depth and seg probing tasks, with an upward trend in quality in the initial layers and a downward trend in the deeper layers, as shown in Fig. 3. Surprisingly, the probes trained to predict the features from \mathbf{E}^{gen} have fairly high cosine similarity (greater than 0.7) for all layers with some irregularities. We attribute the mentioned phenomenon to the choice of CLIP-based [49] \mathbf{E}^{gen} that already has language-aligned features, unlike $\mathbf{E}^{\text{depth}}$ and \mathbf{E}^{seg} .

Visual Encoding Approach. As shown in the first row of Fig. 3, the probes for multi-encoder MLLM learn better representations than the probes for the single-encoder MLLM. Interestingly, for the former, the depth and seg probe performance remain at the same level till layer 20 and then follow a downward trend, indicating the possibility of the deeper layer representations becoming text-rich in deeper layers [39]. We do not observe a downward trend for gen probing, owing to the text-aligned target gen features. We also train probes on our OLA-VLM and observe that they fall between the two baselines, serving as a good trade-off between efficiency and visual representation accuracy.

Training Data. We study the effect of scaling training data on the visual representation quality inside the single-encoder MLLM in the second row of Fig. 3. We analyze four model categories: (i) PT: model after the PT stage, (ii) PT + 50% IFT: model with complete PT and trained on only 50% of the IFT data, (iii) PT + IFT: model with complete PT and IFT, and (iv) PT + VPT + IFT: model with an extra training stage on ALLaVA-Caption [6] data, during which the whole model is trained (see Sec. 5 for more details). We observe that with an increase in the amount of training data for the probed model, the probes show a gradual improvement, indicating that the representations of the visual world inside MLLMs and, consequently, performance on downstream tasks improve with just natural language supervision on more data (Fig. 2a)!

For experimental completeness, we also report probing for the single-encoder LLaVA-1.5 model trained with additional ALLaVA-Caption [6] data during the PT stage. As illustrated in the third row of Fig. 3, while the inclusion of additional PT data improves LLaVA-1.5’s performance on

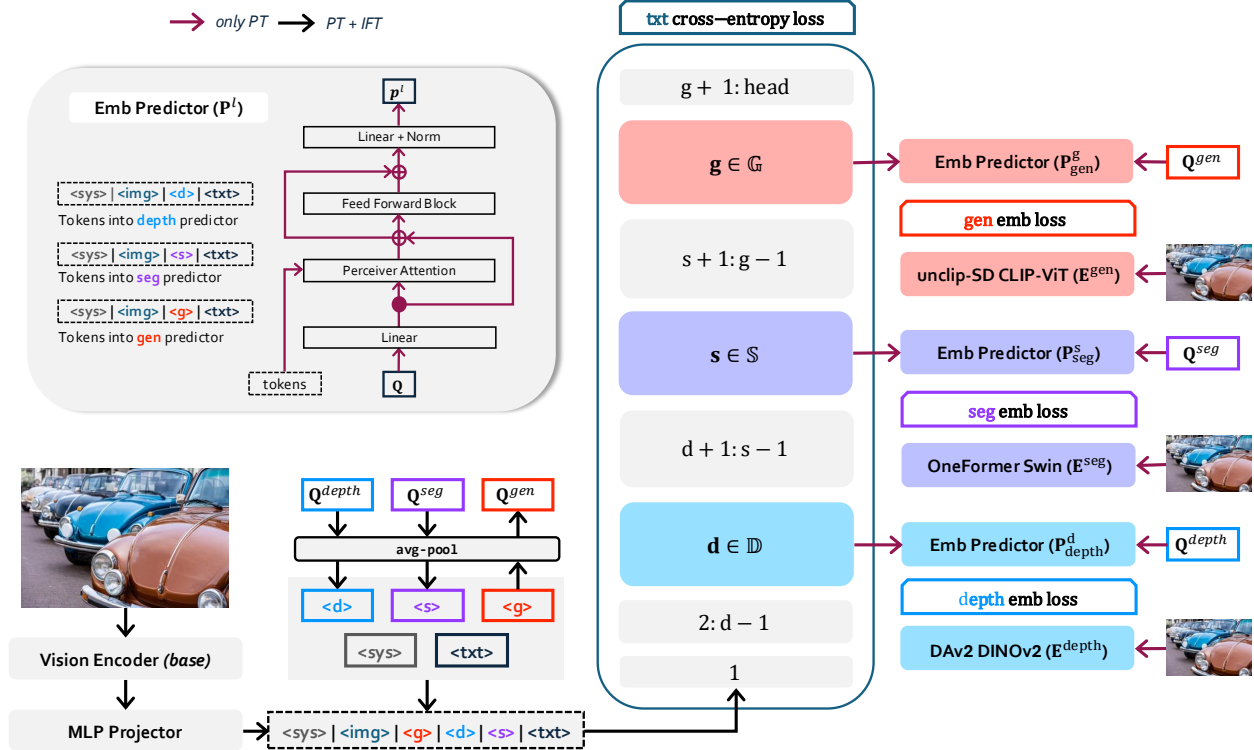


Figure 4. **Architecture for OLA-VLM.** During Pre-Training (PT), we optimize an embedding loss at specific layers for each target encoder: layers $d \in \mathbb{D}$, $s \in \mathbb{S}$, and $g \in \mathbb{G}$ for the depth, segmentation, and generation tasks, respectively. We use a resampler-based embedding predictor [28], denoted as $\mathbf{P}_{\text{task}}^l$ at each layer l , to output predictions. Each predictor takes in two inputs: a set of learnable queries (\mathbf{Q}^{task}) and the token sequence from layer l , with special tokens for other tasks omitted. The final loss is the sum of embedding losses across all selected layers and the next-token prediction objective. During IFT, we train with only the next-token prediction objective while keeping the special tokens frozen so as not to affect their task-specific nature.

CV-Bench, our OLA-VLM achieves superior results with lesser PT data, highlighting the effectiveness of our embedding optimization technique. Notably, there is a significant improvement in representation quality for the seg probing task with the use of ALLaVA-Caption during PT, which we attribute to the dataset’s detailed captions fostering enhanced alignment [6]. Please refer to Tab. 7 for results on other benchmarks.

4. Embedding Visual Information into LLM

The current trend in developing MLLMs for visual reasoning is gluing vision encoder(s) to an instruction-tuned LLM with a projector and training the network to minimize the cross-entropy loss for classification over the LLM’s vocabulary for next token prediction (NTP). In our attempt to add a vision perspective to training MLLMs, we aim to optimize a predictive visual embedding objective for the intermediate LLM layers along with the standard next-token-prediction objective during the PT stage. In other words, we distill auxiliary visual (task) information into the LLM’s intermediate representations rather than feeding the visual features into the LLM from the target encoders. We hypothesize that

such an approach leads to a better projector initialization for the IFT stage. Our hypothesis is validated in Fig. 3, as probes for our OLA-VLM significantly outperform the single encoder baseline, especially in the initial layers. Moreover, we leverage a set of learnable special \mathbf{N}^{seek} tokens ($\langle t \rangle$) to capture task-specific information for each additional representation. The $\langle t \rangle$ are derived from the latent queries input to the corresponding embedding predictor, ensuring the tokens are rich in task-specific information. Therefore, $\langle g \rangle$, $\langle d \rangle$, and $\langle s \rangle$ denote the tokens containing information for gen, depth, and seg tasks, respectively. During IFT, we train the MLLM using only the next-token prediction objective, without any of the embedding predictors, while keeping $\langle g \rangle$, $\langle d \rangle$, and $\langle s \rangle$ in the input sequence to provide the model context about the auxiliary information, resulting in an implicit visual chain-of-thought technique.

4.1. Multi-Encoder Feature Distillation

Given a set of target visual encoders, $\mathbf{E}^{\text{depth}}$, \mathbf{E}^{seg} , and \mathbf{E}^{gen} , our goal is to distill the information from their feature outputs into the LLM’s representation space at specific layers. We solve this challenge by minimizing an embedding loss

between the output of an embedding predictor and the target features at each layer. Since the token sequence inside the LLM has a different length as compared to the target features, we use a single-layer Perceiver Resampler [28] as the embedding predictor ($\mathbf{P}_{\{\text{task}\}}^l$) that takes as inputs the learnable latent queries ($\mathbf{Q}_{\{\text{task}\}}$) along with the token sequence output from layer l of the LLM and outputs a prediction, \mathbf{p}^l . We set the dimension of the $\mathbf{Q}_{\{\text{task}\}}$ such that it matches the dimension of the output from the corresponding $\mathbf{E}_{\{\text{task}\}}$. In our experiments, the number of queries in $\mathbf{Q}^{\text{depth}}$, \mathbf{Q}^{seg} , and \mathbf{Q}^{gen} are 576, 576, and 1, respectively.

To amplify the target information inside the MLLM, we use a set of special \mathbf{N}^{seek} tokens, $\langle t \rangle$ for each task. We append $\langle t \rangle$ to the image tokens in the LLM’s input sequence. Specifically, we average pool $\mathbf{Q}^{\text{depth}}$ and \mathbf{Q}^{seg} into \mathbf{N}^{seek} number of tokens to obtain the $\langle d \rangle$ and $\langle s \rangle$ tokens, respectively. Since the number of target tokens for generation features is only one, we average pool $\langle g \rangle$ to obtain \mathbf{Q}^{gen} . During PT, we only train the MLP projector, embedding predictors, and the special tokens $\langle t \rangle$. We extract the tokens corresponding to the system prompt, input image, the corresponding special tokens ($\langle t \rangle$), and the text query from a layer’s output sequence as the input keys to the embedding predictor. For example, $\mathbf{P}_{\text{depth}}$ takes the token sequence $\{\langle sys \rangle \langle img \rangle \langle d \rangle \langle txt \rangle\}$ as the key input. We present the overview of our OLA-VLM in Fig. 4.

4.2. Predictive Embedding Optimization

At the core of our approach is indirectly optimizing the projector during the PT stage by minimizing an embedding loss for each target representation at specific layers. As shown in Fig. 4, we feed the outputs from the $\mathbb{D} \in \mathbb{D}$, $\mathbb{S} \in \mathbb{S}$, and $\mathbb{G} \in \mathbb{G}$ layers of the LLM into the corresponding embedding predictor to obtain the predictions for computing an embedding loss (\mathcal{L}_{emb}), which is a weighted sum of Smooth-L1-Loss [23] and contrastive (InfoNCE) loss [63]. We denote the sets of layers used to compute embedding losses against target features from $\mathbf{E}^{\text{depth}}$, \mathbf{E}^{seg} , and \mathbf{E}^{gen} as \mathbb{D} , \mathbb{S} , and \mathbb{G} , respectively. The final embedding loss for each target is a sum of losses over all layers from the corresponding layer set. We compute the final loss during PT as the sum of the next-token-prediction objective and embedding losses.

$$\begin{aligned} \mathcal{L}_{\text{sL1}}^l(\mathbf{p}^l, \mathbf{t}) &= \begin{cases} 0.5 \cdot (\mathbf{p}^l - \mathbf{t})^2, & \text{if } |\mathbf{p}^l - \mathbf{t}| < 1, \\ |\mathbf{p}^l - \mathbf{t}| - 0.5, & \text{otherwise.} \end{cases} \\ \mathcal{L}_{\text{contrastive}}^l &= -\log \frac{\exp(\text{sim}(\mathbf{p}_i^l, \mathbf{t}_i)/\tau)}{\sum_{j=1}^B \exp(\text{sim}(\mathbf{p}_i^l, \mathbf{t}_j)/\tau)} \\ \mathcal{L}_{\text{emb}}^l &= \lambda_{\text{sL1}} \mathcal{L}_{\text{sL1}}^l + \lambda_{\text{contrastive}} \mathcal{L}_{\text{contrastive}}^l \\ \mathcal{L}_{\text{emb}}^{\mathbb{D}/\mathbb{S}/\mathbb{G}} &= \sum_{l \in \mathbb{D}/\mathbb{S}/\mathbb{G}} \mathcal{L}_{\text{emb}}^l \\ \mathcal{L}_{\text{PT}} &= \mathcal{L}_{\text{NTP}} + \lambda_{\text{depth}} \mathcal{L}_{\text{emb}}^{\mathbb{D}} + \lambda_{\text{seg}} \mathcal{L}_{\text{emb}}^{\mathbb{S}} + \lambda_{\text{gen}} \mathcal{L}_{\text{emb}}^{\mathbb{G}} \end{aligned} \quad (1)$$

We denote \mathbf{p}^l and \mathbf{t} as the outputs from the embedding predictor ($\mathbf{P}_{\{\text{task}\}}^l$) at layer l and the target task features, respectively, with \mathbf{p}_i^l denoting the i^{th} element in a batch of embeddings with a global batch size of B aggregated over all GPUs. We denote τ (initialized to 2.0) as the learnable scaling factor for the contrastive loss. The weights for smooth-L1 and contrastive losses are $\lambda_{\text{sL1}} = 1$ and $\lambda_{\text{contrastive}} = 0.3$, respectively, at all selected layers. We set the weights for embedding losses, $\lambda_{\text{depth}} = \lambda_{\text{seg}} = \lambda_{\text{gen}} = 0.5$.

Other Architecture Details. As shown in Fig. 4, we use the DINOv2-L [46] from the Depth Anything v2 model [69, 70] as $\mathbf{E}^{\text{depth}}$, the Swin-L [43] from the OneFormer [29] trained on COCO-train2017 [38] set as the \mathbf{E}^{seg} , and the CLIP-ViT-L [19, 49] from the unCLIP-SD-2.1 [50, 53] as the \mathbf{E}^{gen} . In the input sequence to the LLM, we append the gen, depth, and seg special tokens in that order to the image tokens. Therefore, given an image-text pair during training, the input token arrangement is $\{\langle sys \rangle \langle img \rangle \langle g \rangle \langle d \rangle \langle s \rangle \langle txt \rangle\}$, where $\langle sys \rangle$, $\langle img \rangle$, and $\langle txt \rangle$ denote the tokens corresponding to the embedded system prompt, image embeddings, and embedded text query, respectively. The output feature dimensions from \mathbf{E}^{gen} , $\mathbf{E}^{\text{depth}}$, and \mathbf{E}^{seg} are (1, 1024), (576, 1024), and (576, 1536), respectively, corresponding to the final layer outputs of each target encoder.

5. Experiments

In this section, we first provide a comprehensive comparison of our method’s performance to that of the base MLLM, LLaVA-1.5 [41] across different base vision encoder and decoder LLM choices in Tab. 1. Next, we provide experimental results with a 2.5-stage training strategy, composed of an extra Visual Pre-Training (VPT) stage that involves training on the ALLaVA-Caption-663K [6] dataset to demonstrate the scalability of our approach to more data. Lastly, we methodically study various design factors, including the optimal choice of layers for embedding additional visual information and the number of special tokens ($\langle t \rangle$) through a series of ablations.

5.1. Implementation Details

Training. During the PT stage, we use the LLaVA-558K [40, 41] dataset to train our model for an epoch with lr of $1e^{-3}$. We only train the (MLP) projector [41], the embedding predictors, and the special tokens: $\langle g \rangle$, $\langle d \rangle$, and $\langle s \rangle$. During the IFT stage, we use the LLaVA-665K [41] dataset and train the projector and LLM for one epoch with an lr of $2e^{-5}$ while keeping the vision encoder and all the special tokens frozen. When using VPT, we leverage the ALLaVA-Caption-663K [6] dataset to train the whole model (except the special tokens) for one epoch with an lr of $2e^{-5}$. During the PT stage, we train our model with next token prediction and the embedding prediction objectives. During the VPT

Method	Encoder	CV-Bench				General			Avg
		Count ^{2D}	Depth ^{3D}	Relation ^{2D}	Distance ^{3D}	MMStar	RWQA	OK-VQA	
<i>Phi3-4k-mini</i>									
LLaVA-1.5	CLIP-ViT-L	52.4	67.2	75.2	56.3	36.5	57.1	56.7	57.3
OLA-VLM (ours)	CLIP-ViT-L	52.4	68.7	76.0	56.7	36.0	58.0	56.4	57.7
LLaVA-1.5	CLIP-ConvNeXT-XXL	51.8	70.8	74.0	55.3	36.4	58.0	55.9	57.4
OLA-VLM (ours)	CLIP-ConvNeXT-XXL	49.4	72.5	77.2	60.3	38.4	58.4	56.5	58.9
<i>Llama3-8b</i>									
LLaVA-1.5	CLIP-ViT-L	50.4	73.3	64.9	48.7	38.8	57.8	56.9	55.1
LLaVA-1.5 (feat concat.)	CLIP-ViT-L + $E^{\text{depth}} + E^{\text{seg}} + E^{\text{gen}}$	45.3	75.5	70.9	54.3	36.1	57.5	58.3	56.8
LLaVA-1.5 (token concat.)	CLIP-ViT-L + $E^{\text{depth}} + E^{\text{seg}} + E^{\text{gen}}$	45.9	75.7	68.9	52.7	37.8	56.5	59.3	56.7
OLA-VLM (ours)	CLIP-ViT-L	51.3	74.2	69.4	54.3	39.5	57.9	56.6	57.6
LLaVA-1.5	CLIP-ConvNeXT-XXL	54.1	62.8	69.5	49.8	37.4	57.5	56.3	55.3
OLA-VLM (ours)	CLIP-ConvNeXT-XXL	57.4	71.5	66.8	52.8	38.5	55.0	59.0	57.3

Table 1. **Comparisons to Single and Multi-Encoder Baselines.** We present results across different base encoders and decoder LLMs. Our OLA-VLM outperforms the single encoder and multi encoder LLaVA-1.5 [41] by up to 2.5% and 0.9% on average across various benchmarks, respectively. The best numbers are set in **bold** for every base-encoder and decoder LLM combination.

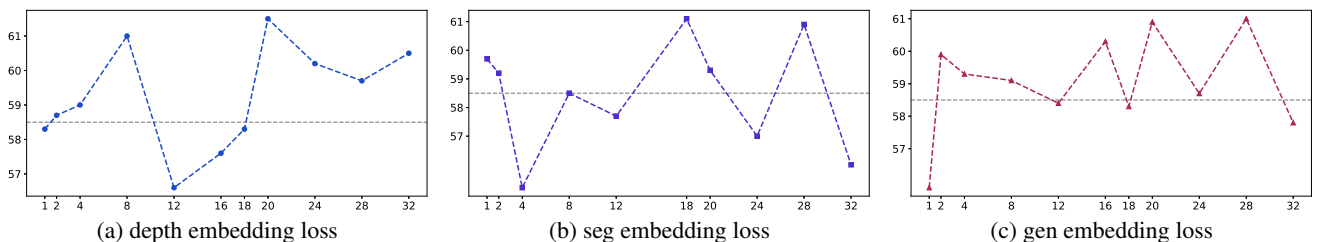


Figure 5. **Ablating choice of layers for \mathcal{L}_{emb} on CV-Bench.** We observe optimal performance by computing the embedding losses for depth, seg, and gen features at the 18th, 18th, and 20th layer, respectively. We do not use any special tokens for this ablation study.

Method	LLM	Count ^{2D}	Depth ^{3D}	Relation ^{2D}	Distance ^{3D}	Avg
LLaVA-1.5	Phi3-4k-mini	49.7	70.0	72.6	58.7	61.8
OLA-VLM (ours)	Phi3-4k-mini	53.7	72.0	73.1	58.5	63.4
LLaVA-1.5	Llama3-8b	56.3	76.8	73.1	50.3	63.3
OLA-VLM (ours)	Llama3-8b	60.0	75.0	70.8	55.2	64.6

Table 2. **Scalability over more data with VPT.** Our OLA-VLM outperforms LLaVA-1.5 on average across different CV-Bench tasks. We use CLIP-ConvNeXT-XXL [13] as the base encoder.

D	S	G	CV-Bench ^{2D}	CV-Bench ^{3D}	MMStar	Avg
{18}	{18}	{20}	58.9	60.9	37.9	52.6
{20}	{18}	{20}	57.6	60.8	38.8	52.4
{8;14}	{10;16}	{12;18}	56.5	56.4	38.8	50.6
{8;20}	{10;18}	{12;20}	58.6	64.2	39.5	54.1
{18;20}	{18;20}	{16;20}	55.8	59.5	40.8	52.0
{16;18;20}	{16;18;20}	{16;18;20}	56.8	61.3	37.0	51.7

Table 3. **Ablations on Layer sets for embedding losses.** Setting $\mathbb{D}=\{8, 20\}$, $\mathbb{S}=\{10, 18\}$, and $\mathbb{G}=\{12, 20\}$ performs the best.

PT	IFT	CV-Bench ^{2D}	CV-Bench ^{3D}	MMStar	RWQA	Avg
single-encoder		56.0	61.0	38.8	57.8	53.4
		57.7	62.9	38.8	57.5	54.2
✓		58.6	64.2	39.5	57.9	55.1
✓	✓	59.1	58.3	38.3	56.2	53.0

Table 4. **Ablations on training stages for embedding losses.** Using the embedding losses only during PT is optimal.

and IFT stages, we only use the next-token prediction objective. Unless mentioned otherwise, we report results with models trained with PT and IFT stages.

We train all our models, including the single and multi-encoder baselines, on 16 AMD 192G-MI300X GPUs with

N^{seek}	CV-Bench ^{2D}	CV-Bench ^{3D}	MMStar	RWQA	Avg
single-encoder	56.0	61.0	38.8	57.8	53.4
0	56.1	62.0	40.1	56.3	53.6
4	60.3	57.9	38.1	56.6	53.2
8	58.6	64.2	39.5	57.9	55.1
12	58.7	60.7	37.9	57.5	53.7
16	56.6	63.6	37.1	54.5	52.9
24	55.7	60.0	39.3	57.4	53.1

Table 5. **Ablations on N^{seek} .** Setting number of special tokens ($\langle t \rangle$) to 8 for each task performs best. The setting with no special tokens ($N^{\text{seek}} = 0$) also outperforms the single encoder baseline.

$\langle t \rangle$ during IFT	CV-Bench ^{2D}	CV-Bench ^{3D}	MMStar	RWQA	Avg
frozen	58.6	64.2	39.5	57.9	55.1
learnable	56.9	56.1	39.0	57.3	52.3

Table 6. **Ablation on the nature of special tokens during IFT.** Keeping $\langle t \rangle$ frozen during IFT aids in keeping their task-specific nature intact, resulting in better performance.

a batch size of 256 during PT and 128 during IFT and VPT. We use CLIP-ViT-L [19, 49] and Llama3-8b [58] as the default base vision encoder and decoder LLM, unless mentioned otherwise. We set N^{seek} to 8 by default. We set \mathbb{D} , \mathbb{S} , and \mathbb{G} to $\{8, 20\}$, $\{10, 18\}$, and $\{12, 20\}$, respectively.

Evaluation. We primarily evaluate OLA-VLM for vision-centric abilities on CV-Bench (Cambrian Vision centric Benchmark) [61] and report results for all four tasks in CV-Bench: *Count* (2D), *Relation* (2D), *Depth* (3D) and *Distance* (3D), for fine-grained understanding of the im-

Method	PT	IFT	CV-Bench ^{2D}	CV-Bench ^{3D}	MMStar	OK-VQA	Avg
LLaVA-1.5	LLaVA-558K	LLaVA-665k	60.0	56.3	37.4	56.0	52.4
LLaVA-1.5	LLaVA-558K + ALLaVA-Caption-663K	LLaVA-665k	56.8	60.8	37.1	57.5	53.1
OLA-VLM	LLaVA-558K	LLaVA-665k	60.8	62.2	38.5	59.0	55.1

Table 7. **Using additional data during PT v/s embedding optimization.** Our OLA-VLM demonstrates superior performance than the LLaVA-1.5 model trained on with additional ALLaVA-Caption [6] data during the PT stage, underscoring the effectiveness of our approach.

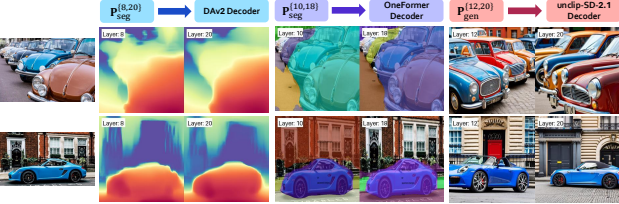


Figure 6. **Visualizing Embedding Predictor Outputs after the PT stage.** The quality of the decoded representations indicates the effectiveness of our embedding optimization.

provements brought about by our embedding optimization. For ablations, we report the average accuracy over the 2D (*count* and *relation*) and 3D (*depth* and *distance*) task categories. We also evaluate our models’ general visual reasoning capabilities on the MMStar [7], RWQA (Real-WorldQA) [66], and OK-VQA [45] benchmarks.

5.2. Main Results

As shown in Tab. 1, our OLA-VLM outperforms the single encoder baseline, i.e., LLaVA-1.5 [41] across different base encoder [13, 19, 49] and decoder LLM [58, 59] combinations. Specifically, Llama3-8b [58] based OLA-VLM outperforms LLaVA-1.5 by **5.6%** and **4.5%** on the *Distance* and *Relation* task, respectively for the CLIP-ViT-L base encoder and by **8.7%** on the *Depth* task for the CLIP-ConvNext-XXL base encoder. Furthermore, we compare our approach to the corresponding two variants of multi-encoder baselines: (i) *feat concat.*: features from all encoders are concatenated along the feature dimension and passed into a single MLP; and (ii) *token concat.*: features from all encoders are first passed through a separate MLP and then concatenated along with token dimension after average pooling the sequence outputs from E^{depth} and E^{seg} into eight tokens each. As shown in Tab. 1, our OLA-VLM outperforms the *feature concat.* and *token concat.* baselines, showing the effectiveness of our approach while only using a single encoder during inference.

Scalability with VPT. We report results with the 2.5 training (PT+VPT+IFT) stages setup for the LLaVA-1.5 [41] and our OLA-VLM in Tab. 2. our OLA-VLM outperforms baseline model on average across all CV-Bench tasks, demonstrating the scalability of our embedding optimization approach with more training data.

5.3. Ablations

Layer Sets for Embedding Losses. The choice of layers in \mathbb{D} , \mathbb{S} , and \mathbb{G} for the corresponding embedding losses is a crucial design choice with a significant effect on the performance. We study the relation between performance and the position of an embedding loss, one layer and loss type at a time for Llama-3-8b [58] in Fig. 5. We find that setting \mathbb{D} , \mathbb{S} , and \mathbb{G} as $\{18\}$, $\{18\}$, and $\{20\}$, respectively results in most optimal performance individually. We also ablate on the choice of layers sets while using multiple embedding losses at the same time. As shown in Tab. 3, setting \mathbb{D} , \mathbb{S} , and \mathbb{G} as $\{8, 20\}$, $\{10, 18\}$, and $\{12, 20\}$, respectively, performs the best overall for the 32-layer Llama3-8b [58].

Training Stage for Embedding Optimization. We observe that adding embedding losses during IFT results in a performance drop compared to using them only during the PT stage, as shown in Table 4. We attribute this to the interference of vision-centric supervision with task-aligned natural language supervision during IFT. Additionally, the second row of Table 4 shows that using learnable tokens in the sequence without embedding loss slightly improves over the baseline but remains inferior to our OLA-VLM.

Number of Special Tokens. We analyze the effect of the number of special tokens per target feature ($\langle t \rangle$) on the performance in Tab. 5. Setting N^{seek} as eight results in the best average performance across benchmarks.

Nature of Special tokens during IFT. As shown in Tab. 6, keeping the special tokens ($\langle t \rangle$) frozen during the IFT stage performs better as compared to making them learnable. We attribute frozen tokens performing better to the gradients from natural language supervision interfering with the vision-centric information stored in the special tokens during IFT if those are set as learnable parameters.

Visualizing Embedding Predictions for Target Tasks. We visualize the visual quality of LLM representations after the PT stage for our OLA-VLM using the decoders from the corresponding target models, as shown in Fig. 6. We observe that the decoder outputs have good object shape and boundary quality, demonstrating the successful representation optimization with our embedding losses.

5.4. Evaluating Probes on Downstream Tasks

We evaluate the probes trained against the target features on the corresponding downstream target tasks, i.e., image generation, depth estimation and image segmentation. To

Probed Model	FID [54] (↓)	DA-2K % Acc. [70] (↑)	% mIoU [29] (↑)
LLaVA-1.5	23.1	66.4	39.3
OLA-VLM (ours)	22.4	77.8	45.4
Target Encoder	18.1	97.3	64.5

Table 8. **Quantitative Evaluation on target probing task.** Probes trained for our OLA-VLM perform significantly better as compared to the probes trained on baseline LLaVA-1.5 [41].

obtain the predictions, we feed the outputs from the probes into the decoder from the corresponding target model. Specifically, we report the FID [54] scores on 5k images from COCO-val2017 [38] for gen probes, accuracy on the DA-2K [70] benchmark for depth probes, and mIoU [29] on the COCO-val2017 [38] set for seg probes. We average the scores over all layers for easier comparison. As shown in Tab. 8, probes trained for our OLA-VLM outperform those for the baseline LLaVA-1.5 [41] model across all probing tasks, proving the improved visual representation quality owing to our embedding optimization approach.

6. Future Work

With OLA-VLM, we enhanced the quality of representations inside the LLM with guidance from target encoders trained for depth, segmentation, and generation tasks. Looking ahead, incorporating more teacher encoders, such as SigLIP [72], and InternViT [10, 11] offer a promising pathway to extend our approach to improving general reasoning abilities. Additionally, applying predictive embedding optimization for low-level information like motion control [4] while training on videos could improve MLLMs’ spatial and temporal reasoning in the future.

7. Conclusion

In this work, we began by probing MLLMs and established a relationship between the quality of visual representations within the LLM and performance. Building on these insights, we introduced OLA-VLM, the first approach to distill knowledge from target encoders into the LLM via predictive embedding optimization during the Pre-Training stage, complementing the next token prediction objective. We validated that our embedding optimization results stronger vision-language alignment before the IFT stage. Through extensive experiments, we demonstrate OLA-VLM’s superiority to the corresponding baselines in terms of both representation quality and performance on vision-centric benchmarks. We hope our work can serve as an inspiration to the community to develop mixed-modality optimization techniques for improving future MLLMs.

Acknowledgements. We extend our heartfelt gratitude to Fangrui Zhu, Reuben Tan, Min Shi, Bhavika Devnani, Fiona Ryan, and Chieh-Yun (Astrid) Chen for their valuable feedback and insightful discussions. We also sincerely

thank the GCR team at Microsoft for their support in resolving frequent infrastructure challenges, which enabled our experimentation. Lastly, we thank the ML Center @Georgia Tech and Microsoft Research for supporting this work.

References

- [1] Jean-Baptiste Alayrac, Jeff Donahue, Pauline Luc, Antoine Miech, Iain Barr, Yana Hasson, Karel Lenc, Arthur Mensch, Katie Millican, Malcolm Reynolds, Roman Ring, Eliza Rutherford, Serkan Cabi, Tengda Han, Zhitao Gong, Sina Samangooei, Marianne Monteiro, Jacob Menick, Sebastian Borgeaud, Andrew Brock, Aida Nematzadeh, Saahand Sharifzadeh, Mikolaj Binkowski, Ricardo Barreira, Oriol Vinyals, Andrew Zisserman, and Karen Simonyan. Flamingo: a visual language model for few-shot learning. In *NeurIPS*, 2022. 1, 2, 3
- [2] Mahmoud Assran, Quentin Duval, Ishan Misra, Piotr Bojanowski, Pascal Vincent, Michael Rabbat, Yann LeCun, and Nicolas Ballas. Self-supervised learning from images with a joint-embedding predictive architecture. In *ICCV*, 2023. 1, 2, 4
- [3] Mohamed El Banani, Amit Raj, Kevis-Kokitsi Maninis, Abhishek Kar, Yuanzhen Li, Michael Rubinstein, Deqing Sun, Leonidas Guibas, Justin Johnson, and Varun Jampani. Probing the 3d awareness of visual foundation models. In *CVPR*, 2024. 3
- [4] Adrien Bardes, Quentin Garrido, Jean Ponce, Michael Rabbat, Yann LeCun, Mahmoud Assran, and Nicolas Ballas. Revisiting feature prediction for learning visual representations from video. *arXiv*, 2024. 1, 4, 9
- [5] Lucas Beyer, Andreas Steiner, André Susano Pinto, Alexander Kolesnikov, Xiao Wang, Daniel Salz, Maxim Neumann, Ibrahim Alabdulmohsin, Michael Tschannen, Emanuele Bugliarello, Thomas Unterthiner, Daniel Keysers, Skanda Koppula, Fangyu Liu, Adam Grycner, Alexey Gritsenko, Neil Houlsby, Manoj Kumar, Keran Rong, Julian Eisenschlos, Rishabh Kabra, Matthias Bauer, Matko Bošnjak, Xi Chen, Matthias Minderer, Paul Voigtlaender, Ioana Bica, Ivana Balazevic, Joan Puigcerver, Pinelopi Papalampidi, Olivier Henaff, Xi Xiong, Radu Soricut, Jeremiah Harmsen, and Xiaohua Zhai. Paligemma: A versatile 3b vlm for transfer. *arXiv*, 2024. 3
- [6] Guiming Hardy Chen, Shunian Chen, Ruifei Zhang, Junying Chen, Xiangbo Wu, Zhiyi Zhang, Zhihong Chen, Jianquan Li, Xiang Wan, and Benyou Wang. Allava: Harnessing gpt4v-synthesized data for a lite vision-language model, 2024. 4, 5, 6, 8
- [7] Lin Chen, Jinsong Li, Xiaoyi Dong, Pan Zhang, Yuhang Zang, Zehui Chen, Haodong Duan, Jiaqi Wang, Yu Qiao, Dahua Lin, et al. Are we on the right way for evaluating large vision-language models? In *NeurIPS*, 2024. 8
- [8] Ting Chen, Simon Kornblith, Mohammad Norouzi, and Geoffrey Hinton. A simple framework for contrastive learning of visual representations. In *ICML*, 2020. 4
- [9] Xinlei Chen and Kaiming He. Exploring simple siamese representation learning, 2020. 4

- [10] Zhe Chen, Jiannan Wu, Wenhai Wang, Weijie Su, Guo Chen, Sen Xing, Muyan Zhong, Qinglong Zhang, Xizhou Zhu, Lewei Lu, Bin Li, Ping Luo, Tong Lu, Yu Qiao, and Jifeng Dai. Internvl: Scaling up vision foundation models and aligning for generic visual-linguistic tasks. *arXiv*, 2023. 9
- [11] Zhe Chen, Weiyun Wang, Hao Tian, Shenglong Ye, Zhangwei Gao, Erfei Cui, Wenwen Tong, Kongzhi Hu, Jiapeng Luo, Zheng Ma, et al. How far are we to gpt-4v? closing the gap to commercial multimodal models with open-source suites. *arXiv preprint arXiv:2404.16821*, 2024. 1, 9
- [12] An-Chieh Cheng, Hongxu Yin, Yang Fu, Qiushan Guo, Ruihan Yang, Jan Kautz, Xiaolong Wang, and Sifei Liu. Spatial-rppt: Grounded spatial reasoning in vision-language models. In *NeurIPS*, 2024. 3
- [13] Mehdi Cherti, Romain Beaumont, Ross Wightman, Mitchell Wortsman, Gabriel Ilharco, Cade Gordon, Christoph Schuhmann, Ludwig Schmidt, and Jenia Jitsev. Reproducible scaling laws for contrastive language-image learning. In *CVPR*, 2023. 3, 4, 7, 8
- [14] Wenliang Dai, Junnan Li, Dongxu Li, Anthony Meng Huat Tiong, Junqi Zhao, Weisheng Wang, Boyang Li, Pascale Fung, and Steven Hoi. Instructblip: Towards general-purpose vision-language models with instruction tuning, 2023. 3
- [15] Wenliang Dai, Nayeon Lee, Boxin Wang, Zhuolin Yang, Zihan Liu, Jon Barker, Tuomas Rintamaki, Mohammad Shoeybi, Bryan Catanzaro, and Wei Ping. Nvlm: Open frontier-class multimodal llms. *arXiv*, 2024. 2, 3
- [16] Timothée Darcet, Maxime Oquab, Julien Mairal, and Piotr Bojanowski. Vision transformers need registers, 2023. 4
- [17] DeepSeek-AI. Deepseek-v2: A strong, economical, and efficient mixture-of-experts language model, 2024. 1
- [18] Haiwen Diao, Yufeng Cui, Xiaotong Li, Yueze Wang, Huchuan Lu, and Xinlong Wang. Unveiling encoder-free vision-language models. *arXiv preprint arXiv:2406.11832*, 2024. 3
- [19] Alexey Dosovitskiy, Lucas Beyer, Alexander Kolesnikov, Dirk Weissenborn, Xiaohua Zhai, Thomas Unterthiner, Mostafa Dehghani, Matthias Minderer, Georg Heigold, Sylvain Gelly, Jakob Uszkoreit, and Neil Houlsby. An image is worth 16x16 words: Transformers for image recognition at scale. In *ICLR*, 2021. 3, 4, 6, 7, 8, 13
- [20] David Eigen, Christian Puhrsch, and Rob Fergus. Depth map prediction from a single image using a multi-scale deep network. In *Advances in Neural Information Processing Systems*, pages 2366–2374, 2014. 2
- [21] Xiaoran Fan, Tao Ji, Changhao Jiang, Shuo Li, Senjie Jin, Sirui Song, Junke Wang, Boyang Hong, Lu Chen, Guodong Zheng, Ming Zhang, Caishuang Huang, Rui Zheng, Zhiheng Xi, Yuhao Zhou, Shihan Dou, Junjie Ye, Hang Yan, Tao Gui, Qi Zhang, Xipeng Qiu, Xuanjing Huang, Zuxuan Wu, and Yu-Gang Jiang. Mousi: Poly-visual-expert vision-language models. *arXiv*, 2024. 2
- [22] Chunjiang Ge, Ziming Wang Sijie Cheng, Jiale Yuan, Yuan Gao, Jun Song, Shiji Song, Gao Huang, and Bo Zheng. Convlava: Hierarchical backbones as visual encoder for large multimodal models. *arXiv*, 2024. 3
- [23] Ross Girshick. Fast r-cnn. In *ICCV*, 2015. 6
- [24] Jean-Bastien Grill, Florian Strub, Florent Alché, Corentin Tallec, Pierre H. Richemond, Elena Buchatskaya, Carl Doersch, Bernardo Avila Pires, Zhaohan Daniel Guo, Mohammad Gheshlaghi Azar, Bilal Piot, Koray Kavukcuoglu, Rémi Munos, and Michal Valko. Bootstrap your own latent: A new approach to self-supervised learning, 2020. 4
- [25] Kaiming He, Georgia Gkioxari, Piotr Dollár, and Ross Girshick. Mask R-CNN. In *Proceedings of the IEEE International Conference on Computer Vision*, pages 2961–2969, 2017. 2
- [26] Kaiming He, Xinlei Chen, Saining Xie, Yanghao Li, Piotr Dollár, and Ross Girshick. Masked autoencoders are scalable vision learners. In *CVPR*, 2022. 2
- [27] Geoffrey Hinton, Oriol Vinyals, and Jeff Dean. Distilling the knowledge in a neural network. In *NeurIPS Deep Learning Workshop*, 2014. 2, 3
- [28] Andrew Jaegle, Sebastian Borgeaud, Jean-Baptiste Alayrac, Carl Doersch, Catalin Ionescu, David Ding, Skanda Koppula, Daniel Zoran, Andrew Brock, Evan Shelhamer, Olivier Hénaff, Matthew M. Botvinick, Andrew Zisserman, Oriol Vinyals, and João Carreira. Perceiver io: A general architecture for structured inputs & outputs. In *ICLR*, 2022. 4, 5, 6
- [29] Jitesh Jain, Jiachen Li, MangTik Chiu, Ali Hassani, Nikita Orlov, and Humphrey Shi. OneFormer: One Transformer to Rule Universal Image Segmentation. In *CVPR*, 2023. 2, 4, 6, 9
- [30] Jitesh Jain, Anukriti Singh, Nikita Orlov, Zilong Huang, Jiachen Li, Steven Walton, and Humphrey Shi. Semask: Semantically masking transformer backbones for effective semantic segmentation. In *ICCVW*, 2023. 2
- [31] Jitesh Jain, Jianwei Yang, and Humphrey Shi. VCoder: Versatile Vision Encoders for Multimodal Large Language Models. In *CVPR*, 2024. 2, 3
- [32] Oğuzhan Fatih Kar, Alessio Tonioni, Petra Poklukar, Achin Kulshrestha, Amir Zamir, and Federico Tombari. BRAVE: Broadening the visual encoding of vision-language models. In *ECCV*, 2024. 2
- [33] Alexander Kirillov, Eric Mintun, Nikhila Ravi, Hanzi Mao, Chloe Rolland, Laura Gustafson, Tete Xiao, Spencer Whitehead, Alexander C. Berg, Wan-Yen Lo, Piotr Dollár, and Ross Girshick. Segment anything. In *ICCV*, 2023. 2, 3
- [34] Bo Li, Yuanhan Zhang, Dong Guo, Renrui Zhang, Feng Li, Hao Zhang, Kaichen Zhang, Yanwei Li, Ziwei Liu, and Chunyuan Li. Llava-onevision: Easy visual task transfer. *arXiv preprint arXiv:2408.03326*, 2024. 1, 3
- [35] Jiachen Li, Xinyao Wang, Sijie Zhu, Chia-wen Kuo, Lu Xu, Fan Chen, Jitesh Jain, Humphrey Shi, and Longyin Wen. CuMo: Scaling Multimodal LLM with Co-Upcycled Mixture-of-Experts. In *NeurIPS*, 2024. 1, 3
- [36] Kenneth Li, Aspen K Hopkins, David Bau, Fernanda Viégas, Hanspeter Pfister, and Martin Wattenberg. Emergent world representations: Exploring a sequence model trained on a synthetic task. In *ICLR*, 2023. 3
- [37] Yanwei Li, Yuechen Zhang, Chengyao Wang, Zhisheng Zhong, Yixin Chen, Ruihang Chu, Shaoteng Liu, and Jiaya

- Jia. Mini-gemini: Mining the potential of multi-modality vision language models. *arXiv:2403.18814*, 2023. 2, 3
- [38] Tsung-Yi Lin, Michael Maire, Serge Belongie, Lubomir Bourdev, Ross Girshick, James Hays, Pietro Perona, Deva Ramanan, C. Lawrence Zitnick, and Piotr Dollár. Microsoft coco: Common objects in context. In *ECCV*, 2014. 4, 6, 9
- [39] Zhihang Lin, Mingbao Lin, Luxi Lin, and Rongrong Ji. Boosting multimodal large language models with visual tokens withdrawal for rapid inference. *arXiv*, 2024. 4
- [40] Haotian Liu, Chunyuan Li, Qingyang Wu, and Yong Jae Lee. Visual instruction tuning. In *NeurIPS*, 2023. 3, 6
- [41] Haotian Liu, Chunyuan Li, Yuheng Li, and Yong Jae Lee. Improved baselines with visual instruction tuning. In *CVPR*, 2024. 1, 2, 3, 6, 7, 8, 9, 13, 14, 16
- [42] Shikun Liu, Linxi Fan, Edward Johns, Zhiding Yu, Chaowei Xiao, and Anima Anandkumar. Prism: A vision-language model with multi-task experts. *TMLR*, 2024. 2, 3
- [43] Ze Liu, Yutong Lin, Yue Cao, Han Hu, Yixuan Wei, Zheng Zhang, Stephen Lin, and Baining Guo. Swin transformer: Hierarchical vision transformer using shifted windows. In *ICCV*, 2021. 4, 6
- [44] Zhuang Liu, Hanzi Mao, Chao-Yuan Wu, Christoph Feichtenhofer, Trevor Darrell, and Saining Xie. A convnet for the 2020s. In *CVPR*, 2022. 3, 4
- [45] Kenneth Marino, Mohammad Rastegari, Ali Farhadi, and Roozbeh Mottaghi. Ok-vqa: A visual question answering benchmark requiring external knowledge. In *CVPR*, 2019. 8
- [46] Maxime Oquab, Timothée Darcet, Theo Moutakanni, Huy V. Vo, Marc Szafraniec, Vasil Khalidov, Pierre Fernandez, Daniel Haziza, Francisco Massa, Alaaeldin El-Nouby, Russell Howes, Po-Yao Huang, Hu Xu, Vasu Sharma, Shang-Wen Li, Wojciech Galuba, Mike Rabbat, Mido Assran, Nicolas Ballas, Gabriel Synnaeve, Ishan Misra, Herve Jegou, Julien Mairal, Patrick Labatut, Armand Joulin, and Piotr Bojanowski. Dinov2: Learning robust visual features without supervision, 2023. 4, 6
- [47] William Peebles and Saining Xie. Scalable diffusion models with transformers. In *ICCV*, 2023. 4
- [48] Alec Radford, Jeff Wu, Rewon Child, David Luan, Dario Amodei, and Ilya Sutskever. Language models are unsupervised multitask learners. *arXiv*, 2019. 1, 3
- [49] Alec Radford, Jong Wook Kim, Chris Hallacy, Aditya Ramesh, Gabriel Goh, Sandhini Agarwal, Girish Sastry, Amanda Askell, Pamela Mishkin, Jack Clark, Gretchen Krueger, and Ilya Sutskever. Learning transferable visual models from natural language supervision. *arXiv*, 2021. 3, 4, 6, 7, 8, 13
- [50] Aditya Ramesh, Prafulla Dhariwal, Alex Nichol, Casey Chu, and Mark Chen. Hierarchical text-conditional image generation with clip latents. *arXiv*, 2022. 2, 4, 6
- [51] Mike Ranzinger, Greg Heinrich, Jan Kautz, and Pavlo Molchanov. Am-radio: Agglomerative vision foundation model reduce all domains into one. In *CVPR*, 2024. 4
- [52] Nikhila Ravi, Valentin Gabeur, Yuan-Ting Hu, Ronghang Hu, Chaitanya Ryali, Tengyu Ma, Haitham Khedr, Roman Rädle, Chloe Rolland, Laura Gustafson, Eric Mintun, Junting Pan, Kalyan Vasudev Alwala, Nicolas Carion, Chao-Yuan Wu, Ross Girshick, Piotr Dollár, and Christoph Feichtenhofer. Sam 2: Segment anything in images and videos. *arXiv preprint arXiv:2408.00714*, 2024. 2
- [53] Robin Rombach, Andreas Blattmann, Dominik Lorenz, Patrick Esser, and Björn Ommer. High-resolution image synthesis with latent diffusion models. In *CVPR*, 2022. 2, 4, 6
- [54] Maximilian Seitzer. pytorch-fid: FID Score for PyTorch. <https://github.com/mseitzer/pytorch-fid>, 2020. Version 0.3.0. 9
- [55] Min Shi, Fuxiao Liu, Shihao Wang, Shijia Liao, Subhashree Radhakrishnan, De-An Huang, Hongxu Yin, Karan Sapra, Yaser Yacoob, Humphrey Shi, Bryan Catanzaro, Andrew Tao, Jan Kautz, Zhiding Yu, and Guilin Liu. Eagle: Exploring the design space for multimodal llms with mixture of encoders. *arXiv:2408.15998*, 2024. 3
- [56] Sirmam Swetha, Jinyu Yang, Tal Neiman, Mamshad Nayeem Rizve, Son Tran, Benjamin Yao, Trishul Chilimbi, and Mubarak Shah. X-former: Unifying contrastive and reconstruction learning for mllms. In *ECCV*, 2024. 2
- [57] Chameleon Team. Chameleon: Mixed-modal early-fusion foundation models. *arXiv*, 2024. 3
- [58] LLaMA-3 Team. The llama 3 herd of models, 2024. 1, 4, 7, 8, 13
- [59] Phi3 Team. Phi-3 technical report: A highly capable language model locally on your phone. *arXiv*, 2024. 8
- [60] Qwen2 Team. Qwen2 technical report. *arXiv*, 2024. 1
- [61] Shengbang Tong, Ellis Brown, Penghao Wu, Sanghyun Woo, Manoj Middepogu, Sai Charitha Akula, Jihan Yang, Shusheng Yang, Adithya Iyer, Xichen Pan, Austin Wang, Rob Fergus, Yann LeCun, and Saining Xie. Cambrian-1: A fully open, vision-centric exploration of multimodal llms. *arXiv*, 2024. 1, 2, 3, 7, 13
- [62] Hugo Touvron, Louis Martin, Kevin Stone, Peter Albert, Amjad Almahairi, Yasmine Babaei, Nikolay Bashlykov, Soumya Batra, Prajjwal Bhargava, Shruti Bhosale, Dan Bikel, Lukas Blecher, Cristian Canton Ferrer, Moya Chen, Guillem Cucurull, David Esiobu, Jude Fernandes, Jeremy Fu, Wenyin Fu, Brian Fuller, Cynthia Gao, Vedanuj Goswami, Naman Goyal, Anthony Hartshorn, Saghar Hosseini, Rui Hou, Hakan Inan, Marcin Kardas, Viktor Kerkez, Madian Khabsa, Isabel Kloumann, Artem Korenev, Punit Singh Koura, Marie-Anne Lachaux, Thibaut Lavril, Jenya Lee, Diana Liskovich, Yinghai Lu, Yuning Mao, Xavier Martinet, Todor Mihaylov, Pushkar Mishra, Igor Molybog, Yixin Nie, Andrew Poulton, Jeremy Reizenstein, Rashi Rungta, Kalyan Saladi, Alan Schelten, Ruan Silva, Eric Michael Smith, Ranjan Subramanian, Xiaoqing Ellen Tan, Binh Tang, Ross Taylor, Adina Williams, Jian Xiang Kuan, Puxin Xu, Zheng Yan, Iliyan Zarov, Yuchen Zhang, Angela Fan, Melanie Kambadur, Sharan Narang, Aurelien Rodriguez, Robert Stojnic, Sergey Edunov, and Thomas Scialom. Llama 2: Open foundation and fine-tuned chat models. *arXiv*, 2023. 1
- [63] Aaron van den Oord, Yazhe Li, and Oriol Vinyals. Representation learning with contrastive predictive coding. *arXiv*, 2018. 6
- [64] Weihang Wang, Qingsong Lv, Wenmeng Yu, Wenyi Hong, Ji Qi, Yan Wang, Junhui Ji, Zhuoyi Yang, Lei Zhao, Xixuan

- Song, Jiazheng Xu, Bin Xu, Juanzi Li, Yuxiao Dong, Ming Ding, and Jie Tang. Cogvlm: Visual expert for pretrained language models. *arXiv*, 2023. 1, 3
- [65] Wenxuan Wang, Quan Sun, Fan Zhang, Yepeng Tang, Jing Liu, and Xinlong Wang. Diffusion feedback helps clip see better. *arXiv*, 2024. 4
- [66] xAI. grok, 2024. 8
- [67] Guangxuan Xiao, Yuandong Tian, Beidi Chen, Song Han, and Mike Lewis. Efficient streaming language models with attention sinks. *arXiv*, 2023. 13
- [68] Yifan Xu, Xiaoshan Yang, Yaguang Song, and Changsheng Xu. Libra: Building decoupled vision system on large language models. In *ICML*, 2024. 3
- [69] Lihe Yang, Bingyi Kang, Zilong Huang, Xiaogang Xu, Jiashi Feng, and Hengshuang Zhao. Depth anything: Unleashing the power of large-scale unlabeled data. In *CVPR*, 2024. 2, 6
- [70] Lihe Yang, Bingyi Kang, Zilong Huang, Zhen Zhao, Xiaogang Xu, Jiashi Feng, and Hengshuang Zhao. Depth anything v2. *arXiv:2406.09414*, 2024. 2, 4, 6, 9, 14
- [71] Sihyun Yu, Sangkyung Kwak, Huiwon Jang, Jongheon Jeong, Jonathan Huang, Jinwoo Shin, and Saining Xie. Representation alignment for generation: Training diffusion transformers is easier than you think. *arXiv*, 2024. 4
- [72] Xiaohua Zhai, Basil Mustafa, Alexander Kolesnikov, and Lucas Beyer. Sigmoid loss for language image pre-training. In *ICCV*, 2023. 3, 9
- [73] Pan Zhang, Xiaoyi Dong, Yuhang Zang, Yuhang Cao, Rui Qian, Lin Chen, Qipeng Guo, Haodong Duan, Bin Wang, Linke Ouyang, Songyang Zhang, Wenwei Zhang, Yining Li, Yang Gao, Peng Sun, Xinyue Zhang, Wei Li, Jingwen Li, Wenhai Wang, Hang Yan, Conghui He, Xingcheng Zhang, Kai Chen, Jifeng Dai, Yu Qiao, Dahua Lin, and Jiaqi Wang. Internlm-xcomposer-2.5: A versatile large vision language model supporting long-contextual input and output. *arXiv preprint arXiv:2407.03320*, 2024. 1
- [74] Xiangyu Zhao, Xiangtai Li, Haodong Duan, Haiyan Huang, Yining Li, Kai Chen, and Hua Yang. Towards semantic equivalence of tokenization in multimodal llm. *arXiv preprint*, 2024. 3
- [75] Deyao Zhu, Jun Chen, Xiaoqian Shen, Xiang Li, and Mohamed Elhoseiny. Minigt-4: Enhancing vision-language understanding with advanced large language models. *arXiv*, 2023. 1, 3
- [76] Fangrui Zhu, Jianwei Yang, and Huaizu Jiang. Towards flexible visual relationship segmentation. In *NeurIPS*, 2024. 2

key input to emb. predictor	CV-Bench ^{2D}	CV-Bench ^{3D}	MMStar	RWQA	Avg
$\langle img \rangle \langle t \rangle$	53.0	54.6	38.4	56.7	50.7
$\langle sys \rangle \langle img \rangle \langle t \rangle$	58.7	63.0	38.8	57.4	54.5
$\langle sys \rangle \langle img \rangle \langle t \rangle \langle txt \rangle$	58.6	64.2	39.5	57.9	55.1

Table I. **Key input to the Embedding Predictor.** Feeding the tokens corresponding to the system prompt, image embeddings, corresponding special tokens, and the text query is optimal.

mode	CV-Bench ^{2D}	CV-Bench ^{3D}	MMStar	Avg
LLaVA-1.5	56.0	61.0	38.8	51.9
depth	58.6	63.5	38.8	53.6
seg	56.2	57.6	38.2	50.7
gen	56.2	65.8	39.3	53.8
depth + seg	58.6	61.8	38.6	53.0
depth + gen	53.6	61.8	38.8	51.4
seg + gen	54.2	60.2	39.3	51.2
depth + seg + gen	58.6	64.2	39.5	54.1

Table II. **Embedding Optimization Modes.** Using the depth, seg, and gen embedding losses at the same time is optimal.

$\langle t \rangle$ order	Count ^{2D}	Depth ^{3D}	Relation ^{2D}	Distance ^{3D}	Overall
LLaVA-1.5	50.4	73.3	64.9	48.7	58.5
$\langle d \rangle \langle s \rangle \langle g \rangle$	49.4	68.7	69.2	56.2	59.9
$\langle d \rangle \langle g \rangle \langle s \rangle$	51.6	72.8	70.3	54.5	61.4
$\langle s \rangle \langle d \rangle \langle g \rangle$	48.7	71.3	65.2	52.5	58.5
$\langle s \rangle \langle g \rangle \langle d \rangle$	46.7	71.3	71.2	50.8	58.9
$\langle g \rangle \langle d \rangle \langle s \rangle$	51.3	74.2	69.4	54.3	61.4
$\langle g \rangle \langle s \rangle \langle d \rangle$	50.9	68.8	70.0	50.5	59.2

Table III. **Order of different special tokens in the input sequence to the LLM.** Appending the gen, depth, and seg tokens (in that order) in the LLM’s input sequence after the image tokens is the optimal setup.

Appendix

In this appendix, we first share additional ablations on the effect of order of different special tokens ($\langle g \rangle, \langle d \rangle, \langle s \rangle$) in the input sequence to the LLM. We also ablate different key input possibilities to the embedding predictor in Appendix A. We use CLIP-ViT-L [19, 49] and Llama3-8b [58] as the base vision encoder and decoder LLM, respectively, for the ablations, unless mentioned otherwise. Next, we provide qualitative analysis from our probing experiments including the effect of substituting image input with equivalent text input to the MLLM in Appendix B.

A. Additional Ablations

Input tokens to Embedding Predictor. As shown in Tab. I, we find that including the tokens corresponding to the system prompt in the key input to the embedding predictor is critical for performance. We attribute it to system tokens having high attention scores and effect on the generation [67]. Therefore, distilling target information into the system tokens is crucial for performance. Moreover, including the text query tokens in the key input to the embedding predictors also results in a slight performance boost.

λ_{depth}	λ_{seg}	λ_{gen}	CV-Bench ^{2D}	CV-Bench ^{3D}	MMStar	Avg
LLaVA-1.5			56.0	61.0	38.8	51.9
0.10	0.10	0.10	60.5	61.3	38.3	53.4
0.25	0.25	0.25	56.3	59.4	37.1	50.9
0.50	0.50	0.50	58.6	64.2	39.5	54.1
0.75	0.75	0.75	57.9	59.4	37.6	51.6
1.00	1.00	1.00	55.8	61.7	38.1	51.9

Table IV. **Embedding Loss weights during PT.** Setting each embedding loss’ weight to 0.5 is optimal.

\mathcal{L}_{sL1}	$\mathcal{L}_{\text{contrastive}}$	CV-Bench ^{2D}	CV-Bench ^{3D}	MMStar	Avg
✓		56.8	62.3	38.3	52.5
✓	✓	58.6	64.2	39.5	54.1

Table V. **Ablations on components of embedding losses.** Using both smooth-L1-loss and contrastive loss to compute the final embedding loss is optimal.

Embedding Optimization Mode. In this ablation study, we evaluate various combinations of embedding losses applied during pretraining (PT). Our results, summarized in Tab. II, reveal that the optimal performance is achieved when all three embedding losses—depth, seg, and gen—are used together. Interestingly, we observe that utilizing only depth or gen embedding losses still leads to notable performance improvements, whereas relying solely on seg embedding loss does not yield significant gains. This suggests that different types of target information contribute uniquely to the distillation process. Investigating how the distillation of one type of target information influences the effectiveness of others presents an intriguing direction for future research.

Order of Special Tokens. In Tab. III, we ablate the order of different special tokens in the LLM’s input sequence. We find that $\{\langle g \rangle | \langle d \rangle | \langle s \rangle\}$ and $\{\langle d \rangle | \langle g \rangle | \langle s \rangle\}$ show the best performance on CV-Bench [61]. We choose $\{\langle g \rangle | \langle d \rangle | \langle s \rangle\}$ as our default order due to its performance being better than the baseline on all sub-tasks in CV-Bench.

Embedding Loss weights. In Tab. IV, we ablate on different values of λ_{depth} , λ_{seg} , and λ_{gen} during for the corresponding embedding losses during the pre-training stage. We find that setting each loss weight to 0.5 is optimal.

Effect of Contrastive Embedding Loss. In Tab. V, analyze the impact of the contrastive loss component within the embedding loss. Our findings show that incorporating the contrastive loss significantly enhances performance, highlighting its positive influence on the model’s effectiveness. We keep the smooth L1 loss as a default component to ensure the embedding predictions maintain the same magnitude as the target features, which is crucial for meaningful visualization. **Qualitative Comparisons.** We provide qualitative comparisons demonstrating the difference between LLaVA-1.5 [41] and OLA-VLM for the different tasks in CV-Bench in Fig. I, Fig. III, Fig. IV, and Fig. V.

Count (2D)



How many pictures are in the image? Select from the following choices.

- (A) 3
- (B) 2
- (C) 0
- (D) 1

LLaVA-1.5: (C)

OLA-VLM: (D)

Ground-Truth: (D)



How many trees are in the image?? Select from the following choices.

- (A) 2
- (B) 0
- (C) 1
- (D) 3

LLaVA-1.5: (A)

OLA-VLM: (C)

Ground-Truth: (C)

Figure I. **Qualitative Examples for the Count task in CV-Bench.** Our OLA-VLM can accurately predict the presence of one picture and one tree, unlike LLaVA-1.5 [41].

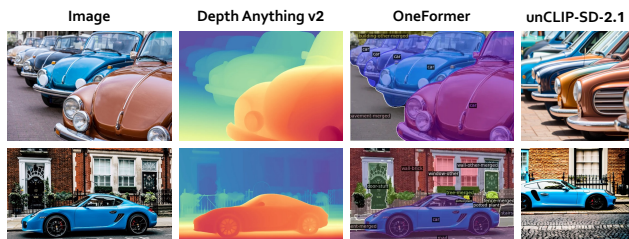


Figure II. Ground-truth outputs from the target models used for Probing MLLMs.

B. Visualizing Probe Outputs

In this section, we present visualizations for the outputs for the probes trained on the single-encoder LLaVA-1.5 model in Sec. 3 in the main text. We provide the ground-truth visualizations from the teacher models in Fig. II.

As shown in Fig. VI, the probe visualizations for the first eight layers of LLaVA-1.5 exhibit blob-like patterns, while the later layers progressively enhance the shape and boundary details of the foreground objects. In contrast, the probe visualizations for our OLA-VLM demonstrate improved object shapes and boundaries starting as early as layer-4, consistent with the findings on representation quality and layer-wise trends discussed in Sec. 3 of the main text. Nevertheless, the visual quality of our probe outputs still lags behind the original Depth-Anything-v2 [70], particularly in accurately representing background objects, as highlighted in Fig. II. Additionally, we present probe visualizations for the segmentation and generative representations

in Fig. VII and Fig. VIII, respectively.

Depth (3D)



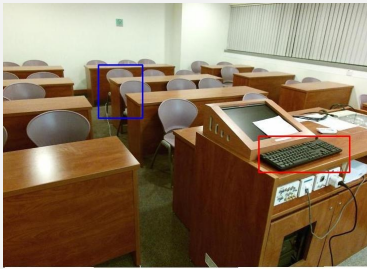
Which object is closer to the camera taking this photo, the lamp (highlighted by a red box) or the books (highlighted by a blue box)?

- (A) lamp
- (B) books

LLaVA-1.5: (A)

OLA-VLM: (B)

Ground-Truth: (B)



Which object is closer to the camera taking this photo, the keyboard (highlighted by a red box) or the chair (highlighted by a blue box)?

- (A) keyboard
- (B) chair

LLaVA-1.5: (B)

OLA-VLM: (A)

Ground-Truth: (A)

Figure III. **Qualitative Examples for the Depth task in CV-Bench.** Our OLA-VLM can accurately predict that the lamp and keyboard are closer to the camera in the respective samples.

Relation (2D)



Considering the relative positions of the trees (annotated by the red box) and the shore in the image provided, where is the trees (annotated by the red box) located with respect to the shore? Select from the following choices.

- (A) above
- (B) below

LLaVA-1.5: (B)

OLA-VLM: (A)

Ground-Truth: (A)



Considering the relative positions of the bottle (annotated by the red box) and the person in the image provided, where is the bottle (annotated by the red box) located with respect to the person? Select from the following choices.

- (A) left
- (B) right

LLaVA-1.5: (A)

OLA-VLM: (B)

Ground-Truth: (B)

Figure IV. **Qualitative Examples for the Relation task in CV-Bench.** Our OLA-VLM can accurately predict that the positions of the trees and the bottle in the respective samples.

Distance (3D)



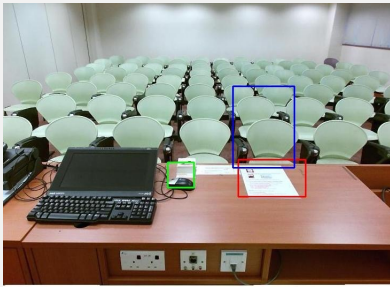
Estimate the real-world distances between objects in this image. Which object is closer to the books (highlighted by a red box), the lamp (highlighted by a blue box) or the table (highlighted by a green box)?

- (A) lamp
- (B) table

LLaVA-1.5: (B)

OLA-VLM: (A)

Ground-Truth: (A)



Estimate the real-world distances between objects in this image. Which object is closer to the stationary (highlighted by a red box), the chair (highlighted by a blue box) or the mouse (highlighted by a green box)?

- (A) chair
- (B) mouse

LLaVA-1.5: (A)

OLA-VLM: (B)

Ground-Truth: (B)

Figure V. **Qualitative Examples for the Distance task in CV-Bench.** Our OLA-VLM can accurately predict that the distances between the respective pair of objects.

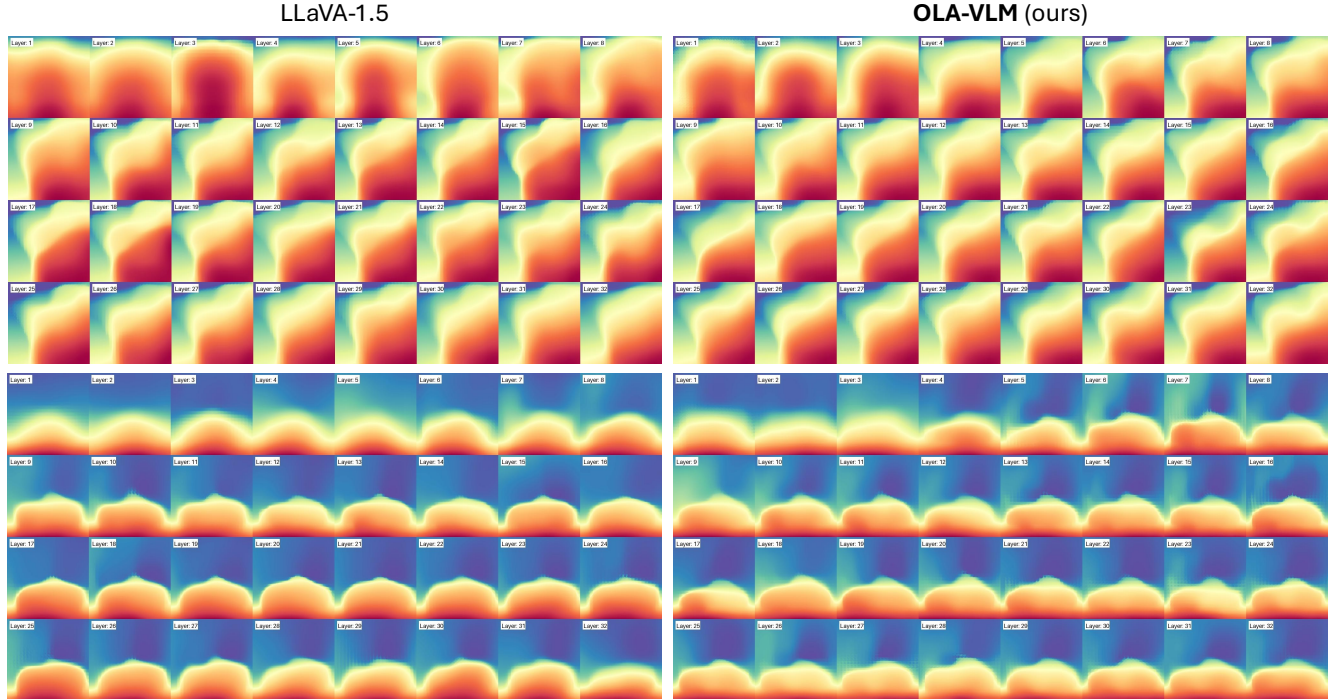


Figure VI. **Layerwise visualizations for the depth probes.** For LLaVA-1.5 [41], the probes generate blob-like outputs up to the eighth layer, with visualizations progressively improving in the middle layers, aligning with the findings presented in Sec. 3 of the main text. Notably, probes trained on OLA-VLM begin producing distinguishable object shapes and boundaries as early as the third layer, attributed to the enhanced projector design and the incorporation of embedding losses.



Figure VII. Layerwise visualizations for the **seg** probes. The LLaVA-1.5 probes often fail to segment the third car in the background for the first sample during the initial layers (layers two to eight), whereas the OLA-VLM probes demonstrate relatively better performance in this scenario. However, for the second sample, both models' probes struggle to segment the background regions effectively, highlighting an opportunity for improvement in future work.



Figure VIII. Layerwise visualizations for the **gen** probes. The probe outputs for both the models are of fairly good quality.